NORSAR

NORSAR Scientific Report No. 2-2009

Semiannual Technical Summary

1 January - 30 June 2009

Frode Ringdal (ed.)

Kjeller, August 2009

6 Summary of Technical Reports /Papers Published

6.1 A climatology of infrasound observations at the experimental ARCI array in Norway

6.1.1 Introduction

Infrasound was first discovered after the violent eruption of the Krakatoa, Indonesia, in 1883. Low frequency pressure waves were observed at traditional barographs. These appeared to have traveled with the sound speed and up to four passages were noticed at some instruments (Symons, 1888). The first microbarometer recordings date from 1908 when a comet, or asteroid, exploded over Siberia in Russia, the so-called Tunguska event. The societal and scientific interest in infrasound increased during World War I, (*e.g.,* Whipple, 1939), and later in the nuclear testing era (Posey & Pierce, 1971). With the signature of the Limited Test Ban Treaty in 1963, most interest in infrasound promptly came to a stop, since nuclear tests were confined to the underground. Only a few studies could be maintained (Balachandran *et al.*, 1977; Liszka, 1978). In recent years, the study of infrasound gained renewed interest with the signature of the CTBT in 1996, where it is used a verification technique for atmospheric tests (Dahlman *et al.*, 2009).

Sources of infrasound are in general large, since an enormous amount of air has to be displaced to generate such low frequencies (Gossard & Hooke, 1975). Natural sources are: avalanches, lightning, meteors, oceanic waves, severe weather, volcanoes, sprites and earthquakes. Among anthropogenic sources are: explosions, supersonic flights, military activity, rocket launches and nuclear tests. Identifying the sources of infrasound out of this zoo of coherent waves in the atmosphere, is one of the major challenges in infrasound research.

The propagation of infrasound through the highly dynamic atmosphere plays an important role in source identification. Infrasound travels up to thermospheric altitudes of 120 km and experiences refractions due to an increase in wind and/or temperature as a function of altitude. If the gradients in the propagation velocity are strong enough, infrasound will be bended back to the earth's surface (Drob *et al.*, 2003). There are three regions in the atmosphere where such gradients might exist. These are of importance in long range sound propagation, *i.e.*, over distances larger than 150 km. The regions are marked by (1) a strong jet stream at 10 km altitude, near the tropopause, (2) the combined effect of wind and temperature at the stratopause, around 50 km altitude and (3) the temperature increase in the thermosphere from 100 km and upwards.

The aim of this study is to identify the sources around the ARCES infrasound and to build up a climatology of station specific detections. Each infrasound array has its own detection capabilities as the atmospheric conditions and source characteristics are highly variable as function of geographical location and time.

6.1.2 The ARCES infrasound array (ARCI)

A temporary, experimental three-element infrasound array was established at ARCES in March 2008, which will be abbreviated as ARCI (Roth *et al.*, 2008). Purpose of the installation is to gain experience with simultaneous recording of seismometer and microbarometer data using minimal wind noise reduction equipment. Fig. 6.1.1 shows the location and configuration of ARCI. The instruments are microbarometers of type MB2005 which have a flat frequency

response to pressure in the range of 0.02 to 10 Hz. Infrasound measurements are affected by noise due to wind. Therefore, a spatial filter is applied at each instruments which essentially integrates the pressure field. Doing so, pressure fluctuations with a small coherency length, like those of tens of centimeters associated with wind noise, are partly canceled out. The infrasonic waves of interest remain undisturbed because of their much larger coherency length of tens to hundreds of meters. Such analog filters can consist of pipe array with discrete inlets, wind barriers or porous hoses (Hedlin *et al.*, 2003). The latter approach is applied at ARCI with four soaker hoses, each with a length of 12 meters, connected to the MB2005. For one of the three sites, the hoses are additionally held centered inside a 5 cm drainage pipe. Environmental restrictions at the ARCES array prevent installation of larger pipe arrays that require fences.

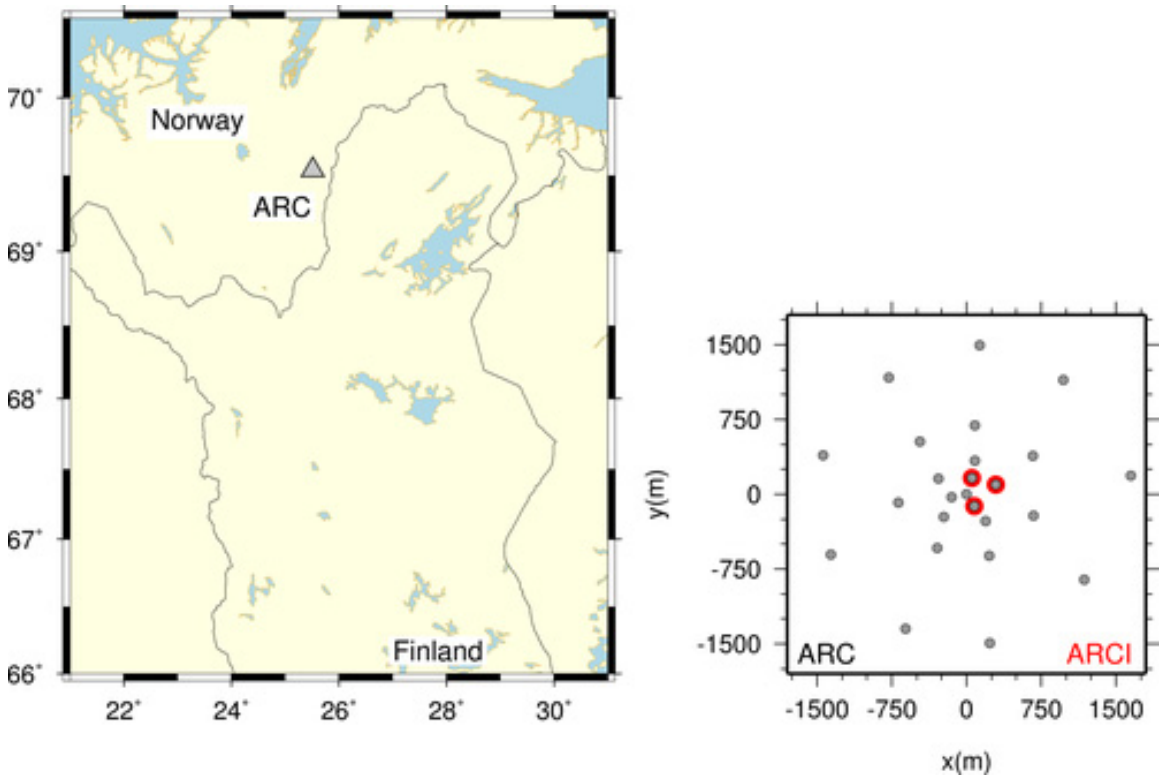

Fig. 6.1.1. The location of the ARCES (ARC) array and positions of the seismometers (gray dots). The temporary array ARCI is configured with three microbarometers (red dots), which are co-located with seismometers in the center of the seismic array.

The temporal resolution of the array is controlled by the sampling rate, leading to a Nyquist frequency which is the highest recoverable frequency given by this digitization in time. Frequencies higher than the Nyquist frequency will be aliased. ARCI is sampled at 80 Hz which means frequencies up to 40 Hz can be resolved. Similarly, the spatial resolution of the array is determined by the configuration and also limited by aliasing. A source cannot uniquely be identified if this so-called spatial aliasing occurs. An infrasound array consists of a limited number of microbarometers in a certain aperture. The reconstruction of the wavefield is affected by this spatial discretization since the atmosphere is not sampled infinitely. In practice, the sensors within an array are placed such that array response approximates a delta function around the desired slowness.

Fig. 6.1.2 shows the array response of ARCI to a monochromatic planar wave of 0.2 and 2.0 Hz, as function of slowness. The main lob is slightly asymmetric which means the array has a

somewhat higher resolution for energy coming from the southwest-northeast direction. Furthermore, side lobs occur at higher frequencies which may lead to spatial aliasing because of the limited sampling of the atmosphere by three microbarometers (Evers, 2008).

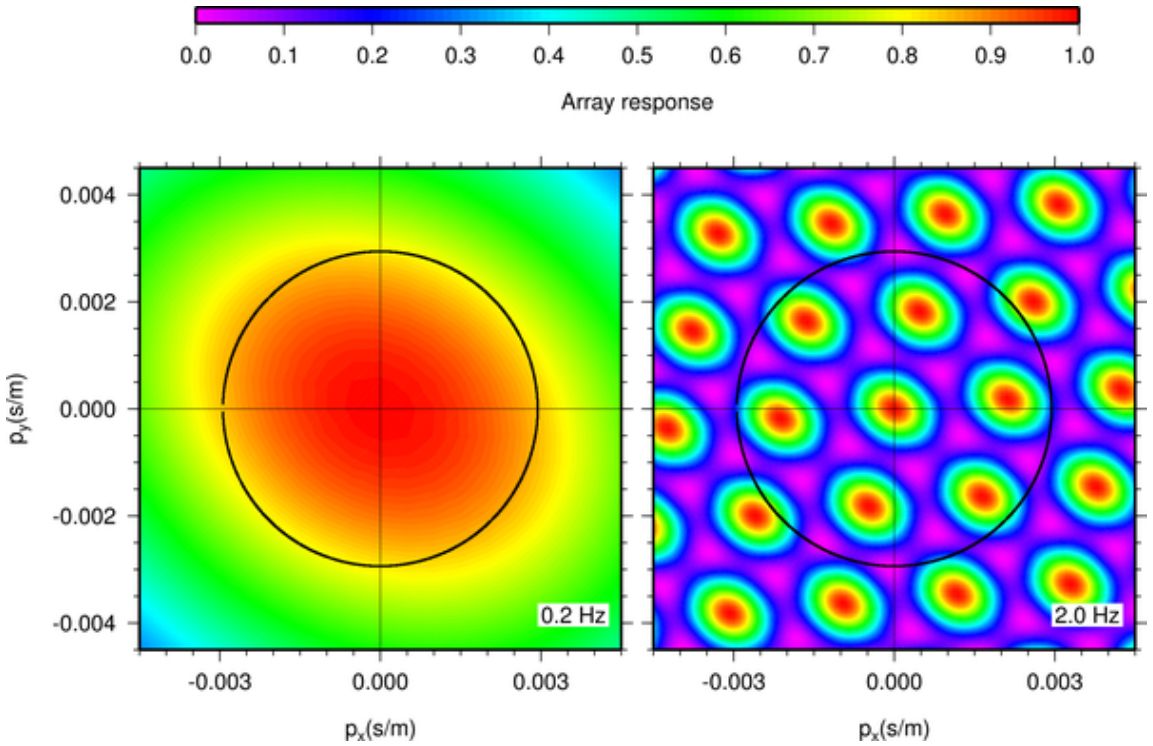

Fig. 6.1.2. The array responses to a monochromatic planar wave of 0.2 Hz (left) and 2.0 Hz (right), as function of slowness. The black circle represents an apparent sound speed of 340 m/s. The broadening of the main lob and occurrence of side lobs is caused by the limited sampling of the atmosphere by three microbarometers. Ideally, the array response would be a delta function which means the atmosphere could be sampled infinitely.

6.1.3 Array processing of infrasound recordings

The detection of coherent infrasonic signals traveling over the array can be achieved by evaluating the Fisher (F) ratio. In essence, a statistical hypothesis is tested. Applying a F-detector is attractive because of its well-known statistical distribution. The hypothesis to be tested is that all recordings made by the microbarometers consist of uncorrelated noise. The alternative hypothesis is valid for the case that not only noise is present but also signal. Evaluated are the variance of the noise and the variance of all recordings, which can not be attributed to the noise since it is common to all signals (Evers, 2008). The F-detector has been described in both the time (Melton & Bailey, 1957) and frequency domain (Smart & Flinn, 1971) and has successfully be applied in infrasound processing to detected, for example, meteors and microbaroms (Evers & Haak, 2001).

The processing sequence applied in this study is as follows:

- Remove the mean of the recordings
- Band-pass filter with a second order Butterworth filter with corner frequencies of 0.1 and 1.0 Hz (the low frequency or microbarom band) and 1.0 and 7.0 (the high frequency band)

- Decimate the data with a factor of 4, to reduce the data volume in order to minimize the computational efforts, from a 80 to 20 Hz sampling rate
- Define a slowness grid of 100x100 point between -0.005 and 0.005 s/m, forming 10,000 beams
- Split the data in segments of 256 samples, which equals a bin of 12.8 seconds
- Evaluate the Fisher ratio for each beam in each bin (with 50% overlapping bins)
- Extract the slowness value, *i.e.*, the back azimuth and apparent sound speed, at the maximum Fisher ratio, for each bin.

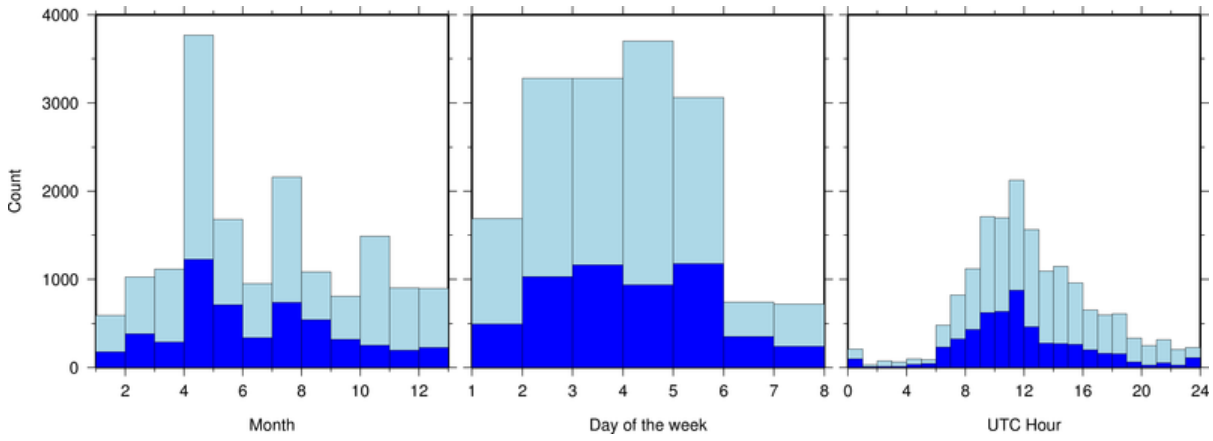

Fig. 6.1.3. Results from the array processing of ARCI data in the high frequency band of 1.0 to 7.0 Hz. The histograms shows the time of occurrence of infrasound events, between 2008, March 13 and 2009, May 14. Light blue colors indicate events with an Signal-to-Noise Ratio (SNR) larger than one (or Fisher ratio of 4 and higher). A total of 16,475 events are detected. Dark blue colors corresponds to SNRs larger than 1.5 of which 5,395 events were detected. The weekday diagram starts with day 1 which is Monday. For the hour histogram, local time in Norway is UTC+2h for summer and UTC+1h for winter.

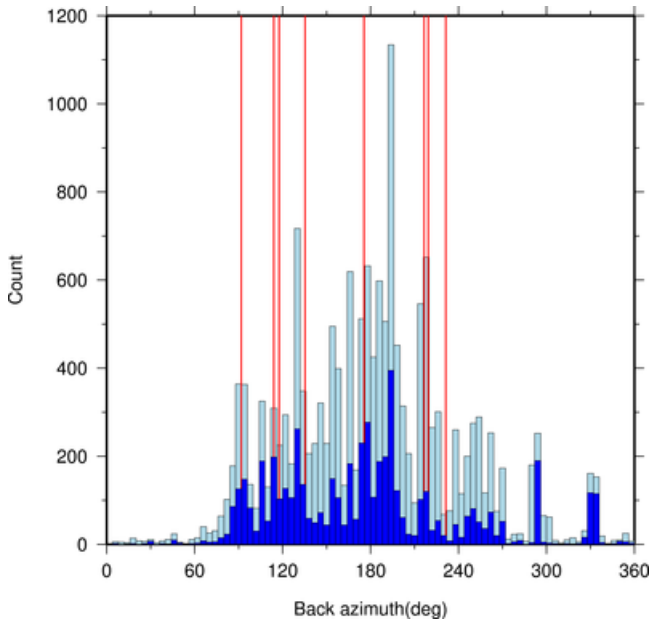

Fig. 6.1.4. The number of events (count) as function of the back azimuth for the high frequency band. Events with a SNR larger than one are denoted by light blue, dark blue is used for and SNR larger than 1.5. The red lines give the back azimuths towards quarries, mines and region of military activity.

Most sources in the high frequency band are man-made. Fig. 6.1.3 shows the time of occurrence of events in this band, for the period of 2008, March 14 up to 2009, May 14. There appear to be less events during the weekends (day 6 and 7) and during nighttime. In other words, most events occur during the working week and at daytime hours, which clearly indicates that the sources are of anthropogenic origin. The resolved back azimuths with respect to ARCI are given in Fig. 6.1.4. Most events occur from a eastern to southwestern direction. Some of these can be explained by quarries, mines and military activity, as indicated by the red lines. Less events find their origin in the the north, although, two distinct peaks, around 290 and 330 degrees, indicate activity to the northwest.

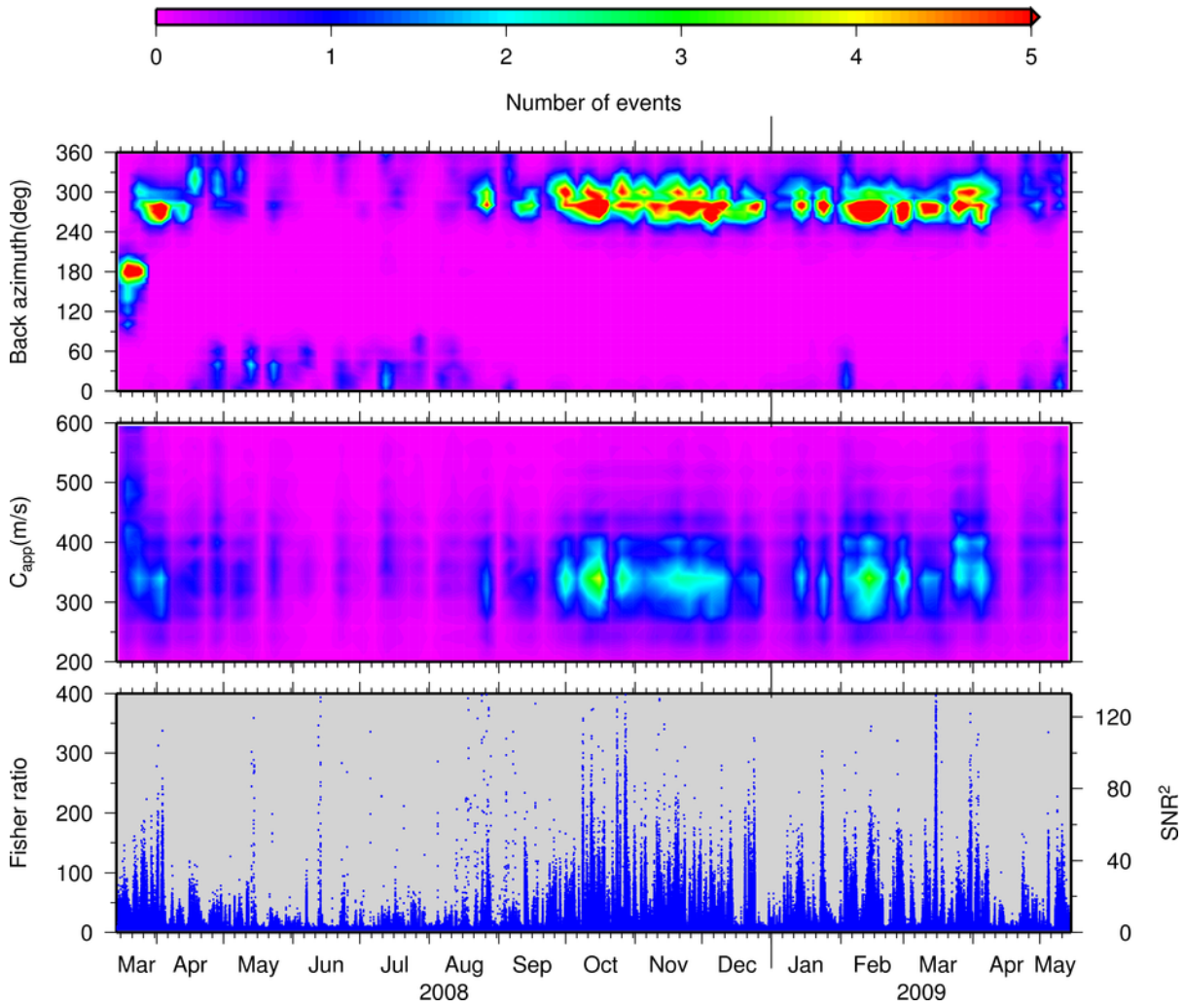

Fig. 6.1.5. Results from the array processing of ARCI data in the low frequency band from 0.1 to 1.0 Hz. The lower frame shows the Fisher ratio as function of time, that is, between 2008, March 13 and 2009, May 14. The Fisher ratio is related to the squared SNR on the traces (see the axis on the right). The top frames gives the resolved apparent sound speed and back azimuth. Color coded are the number events per hour with a SNR larger than one. Five or more events are indicated by red colors. Over the whole timespan, a total of 1.8 million detections were made with a SNR larger than one.

The low frequency band of 0.1 to 1.0 Hz is of utmost importance for the verification of the CTBT as small sized nulcear test (~1 kT TNT) are expected to generate infrasound of 0.1 to 0.2

Hz. It is also this band in which the almost continuous background noise of microbaroms is present, that peak around 0.2 Hz (Posmentier, 1967).

Fig. 6.1.5 shows the results of the above processing approach for ARCI data of 2008, March 14 up to 2009, May 14, for the low frequency band between 0.1 and 1.0 Hz. The lower frame shows the maximum Fisher ratio for each bin. This value is related to the squared Signal-to-Noise Ratio (SNR) on the traces (see axis on the right). The middle and top frame show the resolved apparent sound speed and back azimuth. Color coded are the number of detections within an hour, where five or more detections are denoted by red. Here, only detections with a SNR larger the one are plotted, which equals a Fisher ratio of four and higher. Such a detection will be labeled as an event and are mostly related to microbarom activity.

It follows from the lower frame of Fig. 6.1.5, that signal coherency strongly fluctuates as function of time. Large changes are seen from day to day but there also seems to be a difference between winter and summertime (May to September). These are also reflected in the resolved apparent sound speed and back azimuth. The short time variations in signal coherency show up as gaps, which means no events detected. During summer, less events are detected than in winter and they appear from an eastern directions. In winter, events are detected almost continuously and find their origin to the west of ARCI.

Variations in the detectability of infrasound can have several causes. These could be related to the state of the atmosphere and variations of the source. For the atmosphere, contributions along the source-receiver path will be evaluated in the following and also near receiver effects. The location, time and strength of the source will vary as function of time and will also be analyzed.

6.1.4 The contributions of the atmosphere

Atmospheric causes of the variations in the detectability of infrasound are related to two distinct areas in the atmosphere, the stratosphere and the boundary layer. The boundary layer is approximately the first kilometer of atmosphere, within the lower troposphere. The stratosphere reaches from the tropopause, around 10 km, up to the stratopause near 50 km altitude. The thermosphere, from 100 km and upwards, is not considered here, because thermospheric arrivals are strongly attenuated by the highly rarefied upper atmosphere. These are, therefore, not expected to be observed over ranges of over 1000 km (Sutherland & Bass, 2004).

Stratospheric variability

The wind in the stratosphere, called the polar vortex, varies on a seasonal scale. During winter, winds are directed to the east, around the stratopause, at an altitude of 50 km. These winds can reach values up to 150 m/s. In summer, these winds are directed to the west and somewhat less strong, reaching values of 70 m/s. Fig. 6.1.6 shows the wind and temperature near ARCI, at 69.50N, 25.50E, as function of time. The wind is split in a meridional and zonal component. The meridional wind is the south-north component of the wind and has a positive sign when directed to the north. A positive sign for the zonal wind, which is the west-east component, means it is directed to the east. The change in the zonal wind direction around the equinox should be noted, which causes the anisotropy of the medium. The temperature increase, due to presence of ozone, and strong winds around 50 km altitude may lead the refraction of infrasonic waves back to the earth's surface, due to the increase in effective propagation velocity.

Changes in this so-called stratospheric duct are visible in the surface based microbarometer recordings of ARCI.

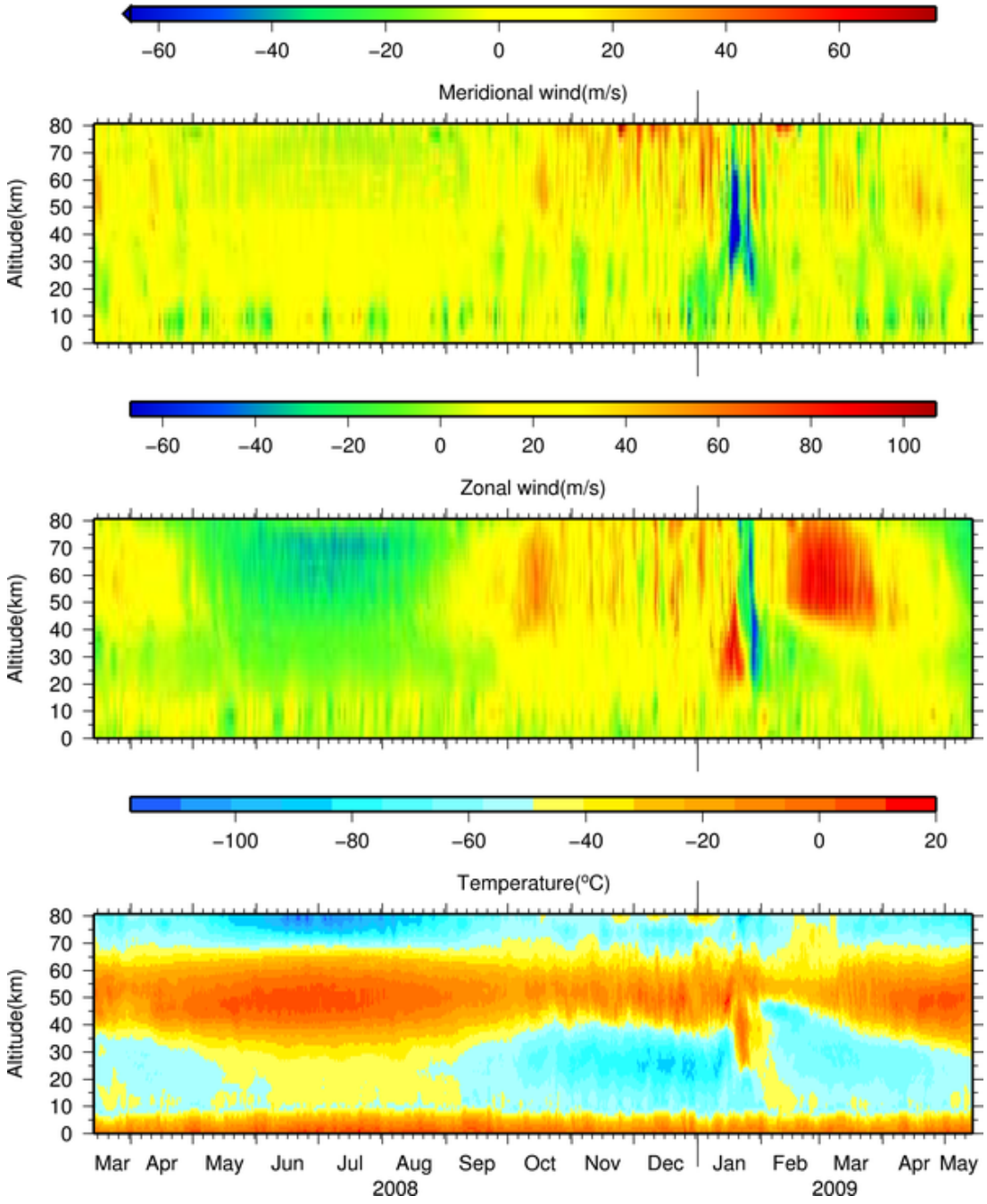

Fig. 6.1.6. The temperature and wind from models provided by the European Centre for Medium-Range Weather Forecasts (ECMWF). These models are available on a 0.5x0.5 deg grid, each six hours per day. The grid node closest to ARCI is chosen, being 69.50N, 25.50E. The wind and temperature is modeled at 91 levels up to approximately 80 km altitude. A positive sign for the zonal wind means it is directed eastwards, i.e., a westerly wind. A positive meridional wind means it is directed to the north. All values for the meridional wind lower than -65 m/s are colored blue, for plotting purposes, the actual lowest value is -140 m/s. An abrupt change in the winds and temperature should be noted in the winter of 2009, between late January and early February. Such changes are related to a major Sudden Stratospheric Warming (SSW).

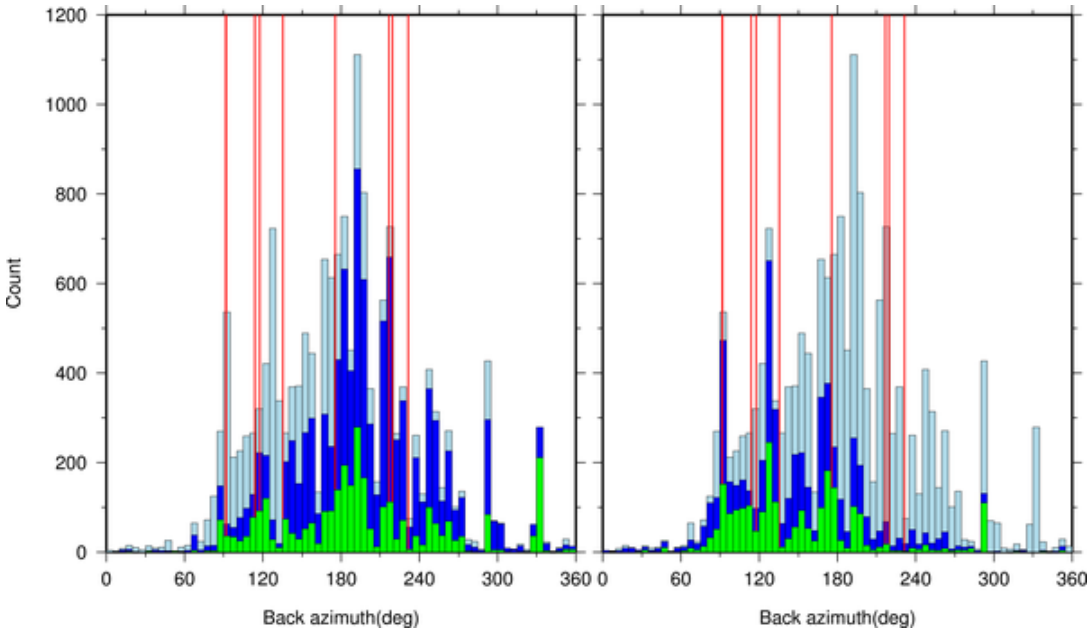

Fig. 6.1.7. The distribution of events in the high frequency band for winter (left) and summer (right). Summer is defined as the period between the equinox in April and September. Light blue colors indicate all detected events, dark blue is used for events in winter and summer with and SNR larger than one, green colors are used for events with and SNR large than 1.5.

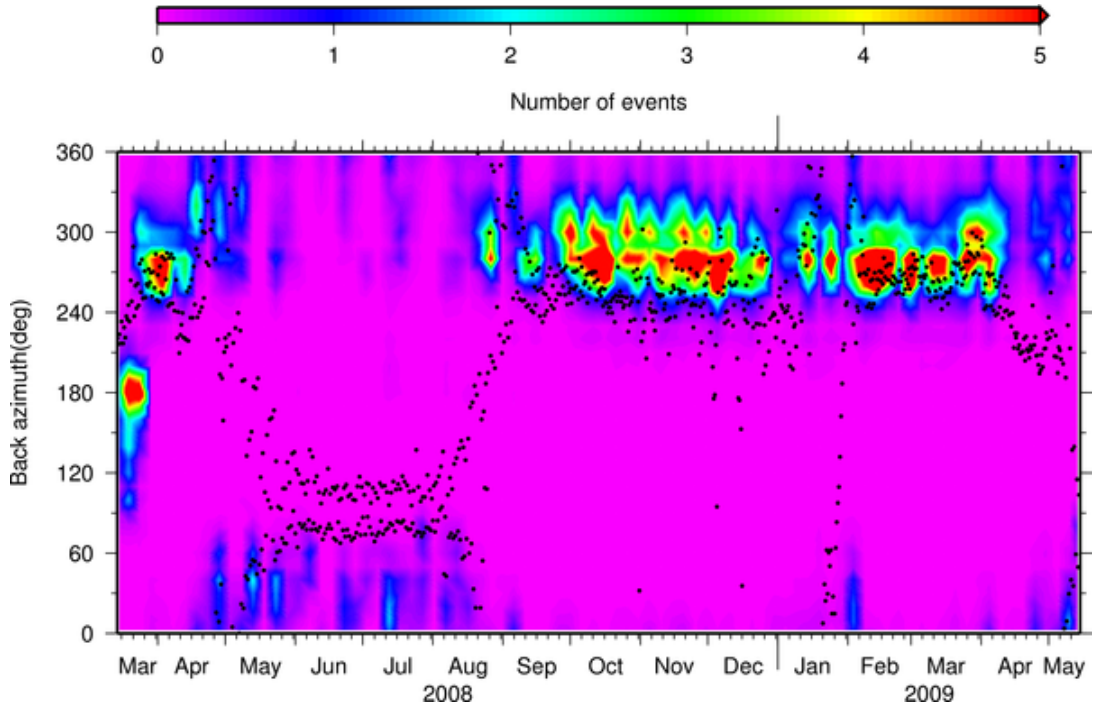

Fig. 6.1.8. The wind direction superimposed on the resolved back azimuths, for the low frequency band. The wind direction is valid for an altitude of 50 km and comes from ECMWF models at 69.50N, 25.5E. The westerly wind in winter changes to an easterly one in summer around the equinox.

For the high frequency band, a distinction is made between summer and winter in Fig. 6.1.7. It follows from this figure, that events from the west are more easily detected in winter as the stratospheric are favorable for such propagation. Events from the east are better detected in summer, but some all show up in wintertime. The detections of sources which are not affected by the direction of the polar vortex probably find their origin close to the array where tropospheric propagation is dominant.

In Fig. 6.1.8, the wind direction at 50 km altitude is superimposed on the resolved back azimuths, for the low frequency band. Clearly, the detection of coherent infrasound is guided by the stratospheric wind. In winter, microbarom energy from the northern Atlantic Ocean is recorded. As the winds turn around the equinox, microbarom energy from the east is being detected.

As can been seen in Fig. 6.1.6, an abrupt change in the winds and temperature occurred in the winter of 2009, between late January and early February. Such changes are related to a major Sudden Stratospheric Warming (SSW). The temperature increases by 50 deg C in the stratosphere, in only a couple of days, and the polar vortex changes direction. The major SSW also had its effect on the infrasound detections (see Fig. 6.1.5). Suddenly, microbaroms from the east are detected because of the change in direction of the polar vortex, which is unusual in winter. To better correlate this observation with the wind, the whole wind field, in three dimensions, should be considered and not just the wind at one grid node.

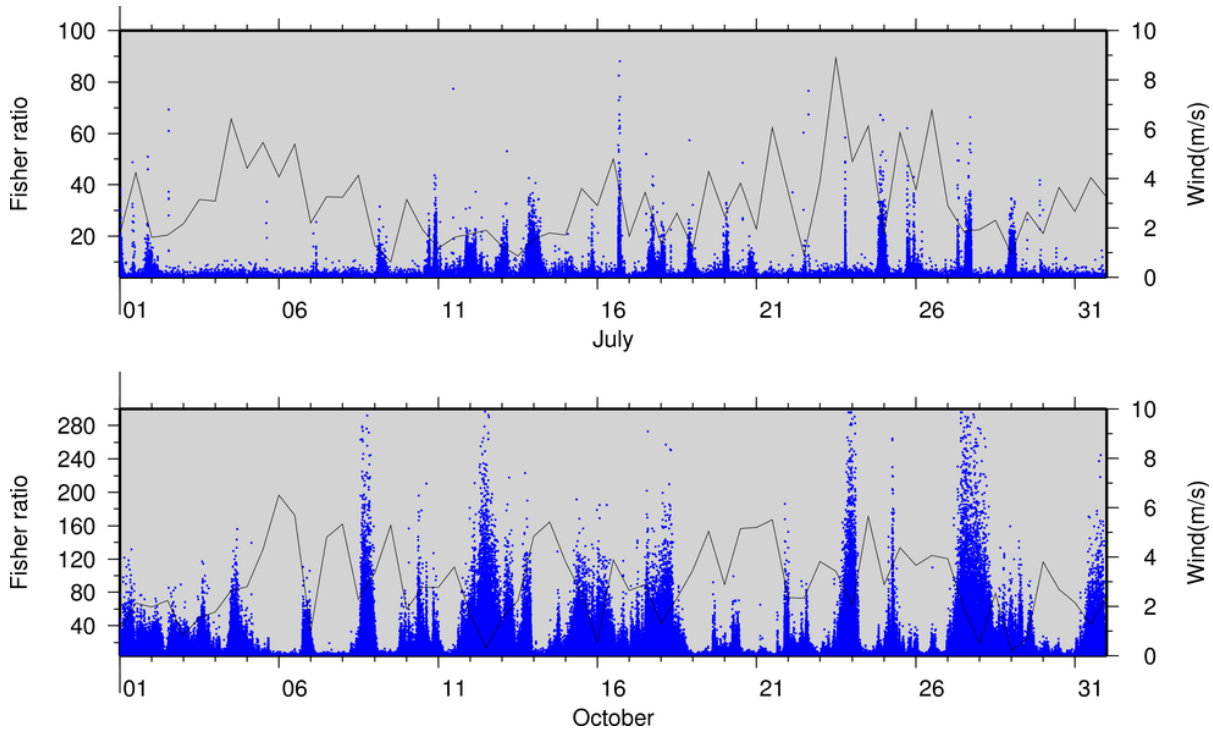

Fig. 6.1.9. The Fisher ratios for 2008, July (top) and October (bottom frame), for the low frequency band. Superimposed are the wind strengths at the first level of the ECMWF models at 69.50N, 25.5E. This first level corresponds to an altitude slightly above the earth's surface.

Variability in the boundary layer

The state of the boundary layer above the array causes de-correlation of the signals. A turbulent atmosphere affects the signal coherency which leads to a decrease of the detection capability. The summer boundary layer is far more turbulent than the winter one. Heating of the boundary layer due to solar radiation generates a high degree of mixing. This effect is also visible on a daily scale where the nighttime boundary layer stabilizes as the influence of solar radiation decreases.

Fig. 6.1.9 shows the signals coherency, by means of the Fisher ratio, for 2008, July and October in the low frequency band. Superimposed are the wind strengths from ECMWF models, at 69.50N, 25.50E, for the first level which is slightly above the earth's surface. It follows from this figure that the wind strength in summer varies on a daily basis. It peaks during daytime and decreases at night when the influence of solar radiation diminishes. The reduction in wind leads to an increase in the detectability of infrasound which is reflected by higher Fisher ratios. Wind variations in winter have longer periods, but also here an increase in wind leads to a decrease in performance of the array.

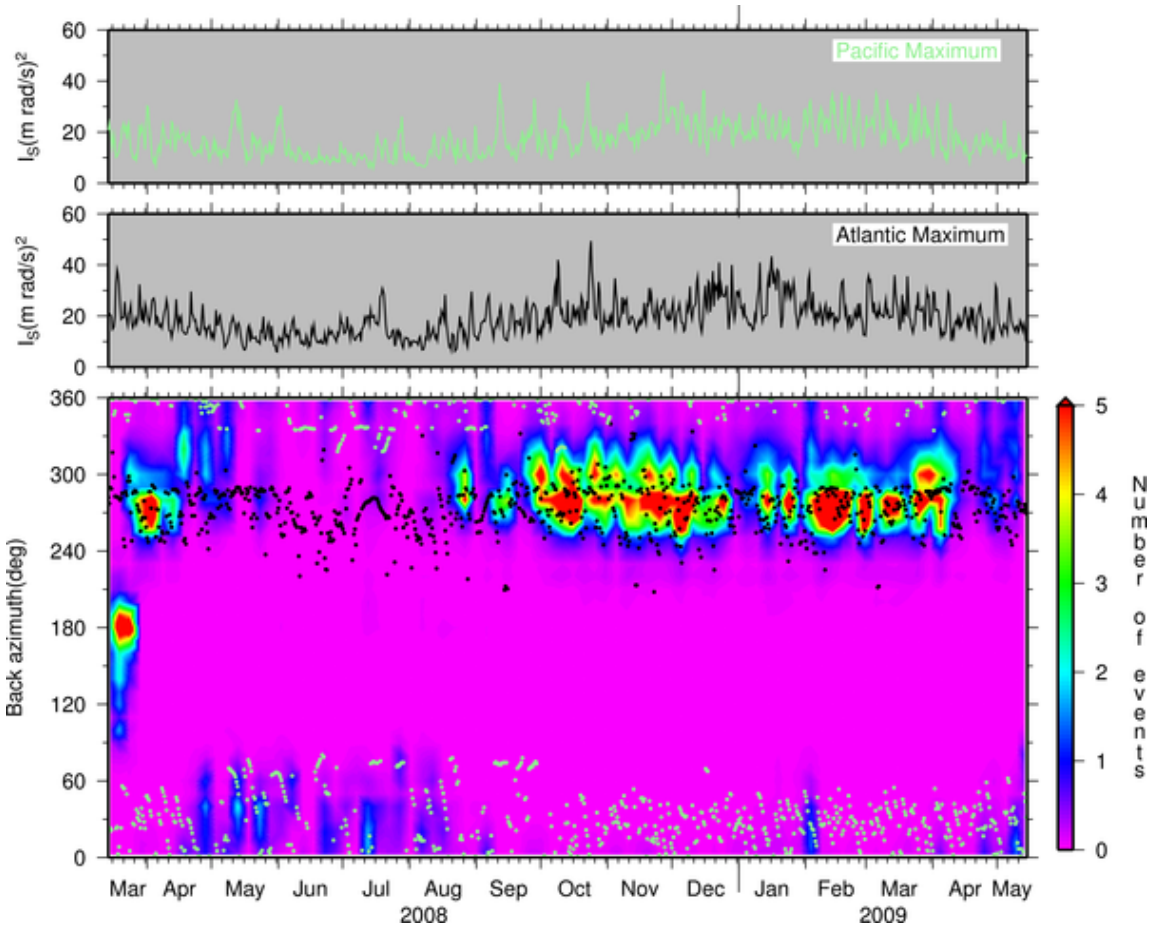

Fig. 6.1.10. An estimate of the microbarom activity in the Atlantic (black) and Pacific Ocean (green dots). The retrieved directions, in the lower frame, and source intensities (I_S, in the upper frames) are calculated from 12-hourly oceanic wave models from ECMWF provided at each 0.5x0.5 deg. As an indicator, the squared multiplication of the wave height and period is taken.

6.1.5 Specifications of the source

The source generating the signals, in the low frequency band, varies in strength over time. The microbaroms are generated by the non-linear interaction of oceanic waves, which often occurs in the vicinity of low pressure systems over the oceans. The interference of almost oppositely traveling waves leads to pressure signals in both the atmosphere and the solid earth, *i.e.* microseism. The signals have a dominant frequency around 0.2 Hz, which is double the frequency of the oceanic waves. The amplitude of induced pressure waves is, in first order, proportional to the squared multiplication of the wave height and frequency. To accurately predict the generation of microbaroms, the directional spectra of oceanic waves should be evaluated to identify the almost oppositely traveling waves and their periods (Kedar *et al.*, 2008). Here, it is assumed that the waves are interacting near the maximum of the squared multiplication of the wave height and frequency. This allows for an efficient calculation, to get an indication of the source activity (Evers & Haak, 2001).

Fig. 6.1.10 shows the back azimuths in the direction of microbarom activity in the Atlantic and Pacific Ocean, from 12-hourly oceanic wave models provided by the ECMWF. The source intensity is also estimated. The observed back azimuths of the infrasound and direction of microbarom activity coincide throughout the seasons The detection of microbaroms is also clearly related to the direction of the stratospheric winds. During the SSW which occurred in the winter of 2009, there is a sudden change in resolved back azimuths. Microbarom energy from the Pacific Ocean is detected, during a short period in early February. This indicates that the low frequency energy detected during summer might also find its origin on the Pacific Ocean.

6.1.6 Discussion and conclusion

Infrasound data from ARCI has been processed by evaluating the Fisher ratio over the period of 2008, March up to 2009, May. Lots of events are detected in both the low and high frequency band. With a detection threshold at a SNR of one, 1.8 million events are detected between 0.1 and 1.0 Hz and 16,475 events between 1.0 and 7.0 Hz. Detections in the low frequency band are mostly related to oceanic wave activity which leads to microbaroms. In the high frequency band, mainly man-made events are detected which are related to mining and military activity.

The characteristics of the medium, *i.e.*, wind and temperature structure up to stratospheric altitudes have been derived from ECMWF models. A clear relation has been shown between upper atmospheric winds and the directionality of the detections for the low frequency band. These seasonal changes are also partly visible in the high frequency band. In winter the sources to the west are detected while preference is given to sources in the east during summer. The state of the boundary layer, or turbulence and low level winds, partly determines the signal coherency. In summer, there is a daily variation caused by the influence of solar radation. A stable boundary layer during nighttime leads to less coherency loss.

In addition, microbarom activity has been estimated by evaluating the ocean wave height and period. ARCI is sensitive to microbaroms from the Atlantic Ocean in winter. Microbarom energy from the east is detected during summer. This anisotropic behavior was also identified during a period of only a couple of days, related to a SWW. A sudden change was noted from the detection of microbarom energy from the Atlantic Ocean to those from the Pacific Ocean.

The importance of taking into account both the characteristics of the medium and source, is illustrated by comparing Fig. 6.1.8 and Fig. 6.1.10. The detections move from west (270 deg) to northwest (330) during 2008, March and April. It follows from Fig. 6.1.10, that the source, microbaroms in the Atlantic Ocean, are occurring with a more or less stable back azimuth between 270 and 300 deg. The stratospheric wind, on other hand, are varying from southwest to north during this period (see Fig. 6.1.8). Therefore, this change in the resolved back azimuths should be attributed to the wind. Another change is visible, in Fig. 6.1.10, between 2008, October and 2009, April. The resolved back azimuth tend to move somewhat from the northwest to the west. The cause should be related to the source, as the wind shows no evidence for such translation. Whether this change relates to the southward movement of sea ice during winter, remains to be investigated.

In conclusion, the general behavior of ARCI can be understood by evaluating the detectability in relation to atmospheric processes and source activity. Upper atmospheric winds and the state of the boundary layer play an important role in the detectability of infrasound. Understanding such dependencies is important for the identification of small-sized nuclear test which are expected to occur in the low frequency or microbarom band.

Läslo G. Evers, KNMI, DeBilt and Delft University of Technology , Delft
Johannes Schweitzer, NORSAR

Acknowledgements

The research visit of Läslo G. Evers at NORSAR was financed by the EC project NERIES (EC Contract Number 026130). Figures in this article were made with the Generic Mapping Tools (Wessel & Smith, 1991).

References

Balachandran, N.K., W.L. Donn & D. Rind (1977). Concorde sonic booms as an atmospheric probe. Science **197**, 47-49.

Dahlman, O., S. Mykkeltveit & H. Haak (2009). Nuclear Test Ban. Springer, Dordrecht.

Drob, D.P., J.M. Picone & M.A. Garcés (2003). The global morphology of infrasound propagation. J. Geophys. Res. **108**, 4680.

Evers, L.G. (2008). The inaudible symphony: on the detection and source identification of atmospheric infrasound. PhD thesis, Delft University of Technology, available at: www.knmi.nl/~evers

Evers, L.G. & H.W. Haak (2001). Listening to sounds from an exploding meteor and oceanic waves. Geoph. Res. Lett. **28**, 41-44.

Gossard, E.E. & W.H. Hooke (1975). Waves in the atmosphere. Elsevier Scientific Publishing Company, Amsterdam.

Hedlin, M.A.H., B. Alcoverro & G. D'Spain (2003). Evaluation of rosette infrasonic noise-reducing spatial filters. J. Acoust. Soc. Am. **114**, 1807-1820.

Kedar, S., M. Longuet-Higgins, F. Webb, N. Graham, R. Clayton & C. Jones (2008). The origin of deep ocean microseisms in the North Atlantic Ocean. Proc. R. Soc. Lond. **A 464**, 777-793.

Liszka, L. (1978). Long-distance focusing of Concorde sonic boom. J. Acoust. Soc. Am. **64**, 631-635.

Melton, B.S. & L.F. Bailey (1957). Multiple signal correlators. Geophysics **XXII**, 565-588.

Posey, J.W. & A.D. Pierce, (1971). Estimation of nuclear explosion energies from micro-barograph records. Nature **232**, 253.

Posmentier, E. (1967). A theory of microbaroms. Geoph. J. R. astr. Soc. **13**, 487-501.

Roth, M., J. Fyen & P.W. LArsen (2008). Setup of an experimental infrasound deployment within the ARCES array. NORSAR Sci. Rep. **2-2008**, 52-59.

Smart, E. & E.A. Flinn (1971). Fast frequency-wavenumber analysis and Fisher signal detection in real-time infrasonic array data processing. Geoph. J. R. astr. Soc. **26**, 279-284.

Sutherland, L.C. & H.E. Bass (2004). Atmospheric absorption in the atmosphere up to 160 km. J. Acoust. Soc. Am. **115**, 1012-1032.

Symons, G.J. (1888). The eruption of Krakatoa and subsequent phenomena. Trübner & Co., London.

Wessel, P. & W.H.F. Smith (1991). Free software helps map and display data. EOS Trans. AGU **72**, 441.

Whipple, F.J.W. (1939). The upper atmosphere, density and temperature, direct measurements and sound evidence. Q. J. R. Meteo. Soc. **65**, 319-323.